PHILOSOPHICAL TRANSACTIONS OF THE ROYAL SOCIETY A MATHEMATICAL, PHYSICAL & ENGINEERING SCIENCES

Multi-Imaging and Multivariate Statistics used for 3D Characterization at Surfaces

M. Prutton, I. R. Barkshire, P. G. Kenny, R. H. Roberts and M. Wenham

Phil. Trans. R. Soc. Lond. A 1996 **354**, 2683-2695
doi: 10.1098/rsta.1996.0123

Multi-imaging and multivariate statistics used for 3D characterization at surfaces

By M. Prutton[1], I. R. Barkshire[1], P. G. Kenny[2], R. H. Roberts[1] and M. Wenham[1]

[1]*Department of Physics, University of York, Heslington, York YO1 5DD, UK*
[2]*Department of Computing, University of Bradford, Bradford BD7 1DP, UK*

Several microanalytical imaging techniques—energy dispersive X-ray detection, parallel electron energy loss spectroscopy, secondary ion mass spectroscopy, photoelectron spectroscopy and XPS) and scanning Auger microscopy—have reached the stage where they are capable of producing images of a surface with a section of a spectrum in each pixel. The resulting *image-spectrum* is a complex data structure which requires the use of special methodologies if the data are to be interpreted effectively. Appropriate methods have been developed for Earth satellite image processing and are directly applicable to surface microanalysis.

The use of scatter diagrams, interactive correlation partitioning, factor and target factor analysis and principal component analysis are outlined in this paper and their application to semiconducting, catalytic and magnetic structures is illustrated. This field of endeavour can be thought of as being the beginning of an area of study which may be called *surface chemometrics.*

1. Introduction

The Landsat satellite which surveys the surface of the Earth contains an imaging system with 57 telescopes viewing the same area of the surface but in different ranges of the optical and near-optical regions of the electromagnetic spectrum. The data produced by this system consist of a set of spatially registered images, each image being formed with scattered light in a different spectral band. This set is an example of what is often referred to as an *image-spectrum*, simply because it contains both spectroscopic and spatial information about the region being viewed. This field of study is reviewed in many image processing monographs (see, for example, Gonzalez & Wintz 1982; Niblack 1986). Interpretation of the set using optical scattering models and multivariate statistical analysis (MSA) results in detailed knowledge as to the identity of materials and their spatial distributions.

Modern methods for the acquisition of images in electron microscopes are analagous to the Landsat system in that they are able to present the experimentalist with image-spectra containing information about the microscopic compositions and spatial distributions of all the chemical phases in the material of the sample. The interpretation of these image-spectra requires the use of models for the electron–solid interaction and MSA. The acquisition of such image-spectra is particularly well developed in the fields of parallel electron energy loss microscopy (or spectroscopy) (PEELS) and secondary ion mass spectrosopy (or microscopy) (SIMS). In PEELS,

Phil. Trans. R. Soc. Lond. A (1996) **354**, 2683–2695
Printed in Great Britain

this development has been dramatic because of the introduction of the imaging spectrometer (Krivanek *et al.* 1990) which has allowed high pixel densities in the images accompanied by good energy resolution (270 meV). In SIMS, the use of time-of-flight mass spectrometers combined with position sensitive detectors has allowed ions with different mass to charge ratios, originating from the same region of the sample, to be collected almost simultaneously (see, for example, Schueler 1990). As the incident ion beam is scanned across a surface, an image set is built up, each component image being formed with ions of a single species. A start has been made on the interpretation of PEELS and SIMS image sets with the aid of MSA and electron (Bonnet 1995) or ion scattering models (Bright *et al.* 1988).

Analytical methods such as Auger electron spectroscopy and scanning Auger microscopy (AES and SAM respectively) for surfaces and energy dispersive X-ray analysis (EDX) for the outer micron or so near to a surface are mature techniques which have also been developed to allow the collection of image-spectra. EDX uses detectors which are inherently capable of parallel data acquisition—many characteristic X-ray energies being detected, stored and displayed at the same time. This is an excellent contender for analysis of image-spectra and although the parallel acquisition has been demonstrated in this way (Browning 1985), it is not yet in widespread use—perhaps because of the absence of suitable computer software on the instruments used to collect the data. AES and SAM are more constrained than EDX in that there is currently no electron spectrometer which is suitable for parallel acquisition of the data required (which commonly spans the range 50–3000 eV). However, it is possible to control a spectrometer to acquire data for different kinetic energies of the scattered electrons sufficiently rapidly that the sample has, for all practical purposes, not moved between the acquisitions. The energy analysed image set so collected is quasi-simultaneous and the MSA methodology can be applied to it. This method has been called (Prutton *et al.* 1991) multispectral Auger microscopy (MULSAM). It has been developed with the exploitation of MSA in mind and so is used here to describe the advantages of this approach by giving specific examples in which it has been valuable.

The objective of this paper is to describe the parts of MSA which have been particularly useful in the interpretation of image sets from the MULSAM instrument. The theory of these methods has been described in detail in the references cited previously and in the literature of MSA (see, for example, Malinowski 1991; Meloun *et al.* 1992) and so only a qualitative explanation is given below.

2. Scatter diagrams

If a set of N images is acquired such that they are spatially registered and each has, say, P by Q image points (pixels) then the N-dimensional histogram of their intensities is a very useful construct. $P \times Q$ points are placed in the histogram. The coordinates of each point are the intensities of that particular pixel in each image in the set. The outcome is a diagram in an N-dimensional hyperspace which contains clusters of points where the pixels in the set of images have the same, or very similar, intensities. The number of clusters gives a measure of the number of different kinds of regions in the area imaged—in the most general sense it describes the number of 'phases' present in this area. The number of points in the cluster expressed as a fraction of $P \times Q$ is a measure of the relative area which is due to that 'phase' within the region imaged. Thus, the scatter diagram provides a means of *classifying*

the number of significantly different regions being imaged and is the first step in the quantitative analysis of the sample.

The word 'phase' is being used here in a very general sense in that it is simply a distinct cluster of points in the scatter diagram which is separated from any neighbouring clusters in a statistically significant manner. For example, one image may be obtained from a secondary electron detector (a SEM image) and the second from the difference in the signals from a backscattered electron detector which provides an image dominated by topographical contrast. The scatter diagram would be two dimensional, because $N = 2$, and the clusters would seperate regions with different angles of incidence to the scanned electron beam because of the topographical sensitivity of the BSE detectors. In this example the 'phases' would be regions with similar angles of incidence. They might, for instance, be different facets of a heavily crystalline rough surface.

Of course, it is impossible to display more than a projection of a 3D scatter diagram ($N = 3$) on a two-dimensional surface such as a visual display unit or a sheet of paper. Therefore, computer algorithms to search an N-dimensional space to find the centres of all the clusters and count the number of pixels in them become critically important for $N > 3$. This subject has been reviewed recently by Bonnet (1995). The difficulties are that an efficient algorithm is essential to search a high-dimensional hyperspace (there may be a very large number of images in a set) and the clusters are often joined by streaks of points— correlation lines. These lines make automatic location of clusters quite difficult. They arise, in part, in the scanned electron beam situation, because the incident electron beam has a finite diameter and it may be located across a sharp edge between two 'phases'. If it spans such an edge then the measured signal from any detector consists of a simple linear combination of the signals from each individual 'phase'. Bonnet describes an evaluation of the so-called 'K-means' method in which the clusters are located by iteration after the analyst has defined preliminary estimates of their centres.

Bright *et al.* (1988) and Kenny *et al.* (1994) describe techniques for the calculation and presentation of 3D scatter diagrams together with means to relate the clusters in the scatter diagrams to the positions in the sample whence the pixels were derived. Because one can view only a 2D projection of a 3D scatter diagram, it is very useful in the display of these diagrams to be able to rotate the presentation so as to inspect the structure of the diagram from different directions. In this way, clusters which may be 'hidden' behind others can be revealed to the observer.

One important use of scatter diagrams is to find how many different 'phases' are present in the data set by locating the cluster centres and to follow this by carrying out spectroscopy at the positions on the sample that correspond to these centres. In this way, the analyst has an objective means of ensuring that spectroscopic information has been obtained for every 'phase' which characterizes that sample. Without this strategy of characterization, there may always be doubt that interesting or unusual 'phases' have been missed by accident.

An example of two views of a 3D scatter diagram is shown in figure 1. The sample was a layer structure (figure 2) which had been fabricated for a microcircuit and was expected to consist of 10 nm of W on 120 nm of TiN on 30 nm of Ti on SiO_2 on Si. A bevel through this structure had been made with a 2 keV Xe^+ ion beam so as to expose a surface at an angle of about 1 mrad to the original surface. With this bevelling technique the depth distribution of the components is exposed on the new surface and can be examined by surface analytical methods. In this case, it was

PHILOSOPHICAL TRANSACTIONS OF THE ROYAL SOCIETY A MATHEMATICAL, PHYSICAL & ENGINEERING SCIENCES

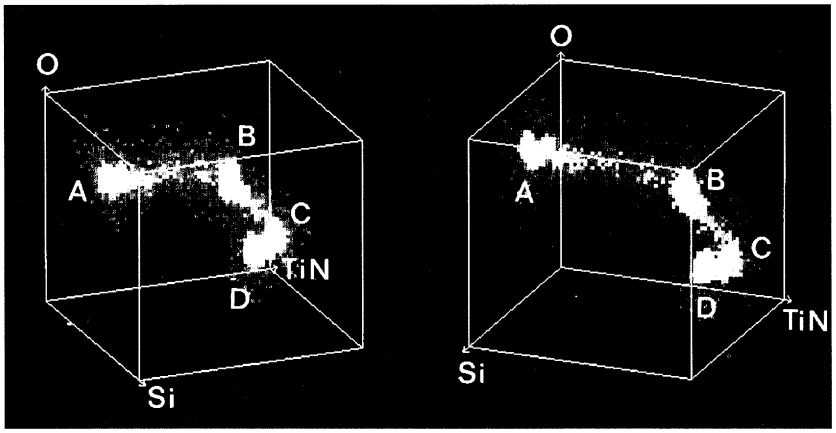

Figure 1. Two projections of the 3D scatter diagram formed from the O, Ti/N and Si peaks described in the text. Clusters A–D contain the largest numbers of pixels and the remaining clusters appear on the correlation streak between clusters A (SiO_2) and B (a mixture of Ti and N peaks)

examined by Auger microscopy in the York MULSAM instrument (Prutton *et al.* 1991). Figure 1 is formed using the Ti, O and TiN Auger peak heights for the region below the W layer and so is expected to contain three clusters corresponding to TiN, Ti and SiO_2. The Auger images in the data set were formed using the O KLL peak at 510 eV, the overlapping Ti and N features at 380 eV and the Si KLL peak at 1610 eV. The scatter diagram reveals four densely occupied clusters, labelled A–D in figure 1, and there are signs of three more less densely occupied clusters situated along the correlation streaks separating the principal clusters. It is immediately clear that the layer structure is considerably more complicated than expected from knowledge of the growth process. Interactive correlation partitioning assists in the interpretation of this structure.

3. Interactive correlation partitioning

In order to reveal the positions in the sample which correspond to the clusters in a scatter diagram it is necessary to delineate each cluster, to assign a colour to those regions of the specimen which map into that cluster and to create a new image which has that colour in the regions which so map. Because the colours chosen in the assignments to each cluster are arbitrary, this part of the operation is often referred to as *false colour imaging*. The whole procedure can be called *interactive correlation partitioning* (ICP). It has the important qualities that each colour in the false colour image represents a different 'phase' in the sample and that information contained in the set of images which form the data has been condensed into a single image. The methodology has been developed in several areas of analytical microscopy. Thus, Browning (1985), El-Gomati *et al.* (1987), Bright *et al.* (1988), King *et al.* (1989), Bright & Marinenko (1992) and Kenny *et al.* (1994) have described applications of this method to backscattered electron, energy analysed electron and X-ray image sets. Bright & Marinenko (1992) applied scatter diagrams and ICP to quantitative multi-element X-ray maps from Cu–Ti alloy and ceramic specimens. They refer to scatter diagrams as composition histogram images and use the term traceback for ICP.

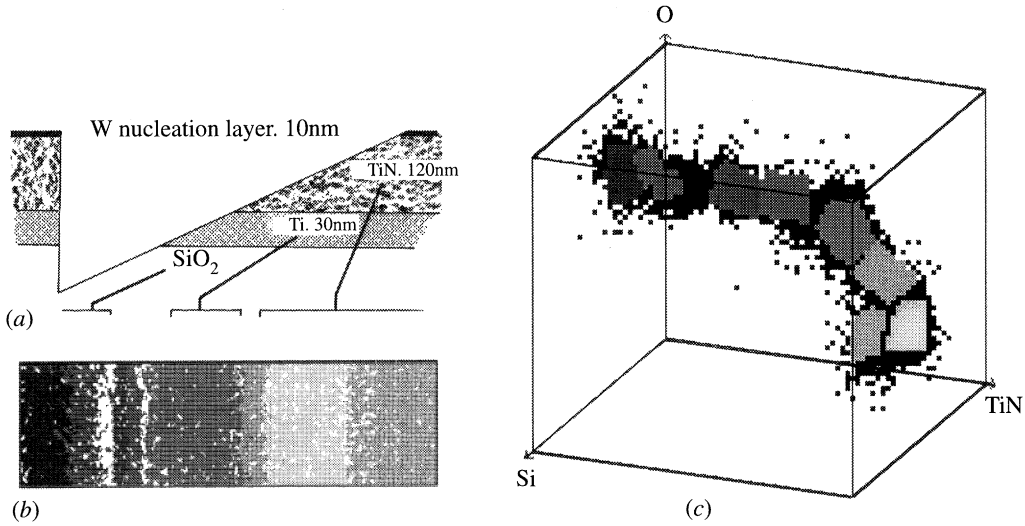

Figure 2. (*a*) Cross-section through the structure which was expected in the sample, the data of which are presented in figures 1 and 3. (*b*) False colour image derived from the scatter diagram of figure 1 together with the scatter diagram which indicates the assignment of false colours to each cluster. Normally the false colour image is in colour but, for reasons of economy, it is reproduced here in a grey scale.

ICP can be applied to the 3D scatter diagram of figure 1 and the result is shown in figure 2, where the tie-lines indicate how each labelled cluster is related to a region in the false colour image. The false colour or 'phase' image can be seen to be layered and the new information obtained is that the various regions identified by the clusters are in distinct thin films situated at the interfaces between the layers which were deposited during the fabrication process.

More information can now be obtained by electron spectroscopy at the cluster centres or at various positions along a line perpendicular to the exposed interfaces between the layers. A set of such spectra are shown in figure 3 for the kinetic energy range spanning the region around the Si LVV peak. Two features in the data are revealed: (a) there are three Si states—at 70, 75 and 89 eV; (b) there are two oxygen states as indicated by the O KLL energies—one at 501 eV and the other at 509 eV (these are not shown in figure 3). These chemical shifts suggest that reactions have occurred between the materials of the layer structure.

Interactive correlation partitioning together with the spectra can now be used to identify the spatial locations of the states revealed in the spectra. The oxygen state at 501 eV is spatially associated with the SiO_2 and that at 509 eV is associated with the Ti. The Si state at 89 eV is spatially associated with the Ti and is at the energy expected for elemental Si. The states at 70 and 75 eV are associated with the SiO_2 and the interfacial region between the Ti and the SiO_2 respectively. The latter may be a chemical state associated with a mixed Ti/Si oxide or perhaps a silicide —further work would be needed to resolve these alternatives. Thus, although it is not surprising that interdiffusion and reaction of the elements of the deposited layers has occurred, this analysis has revealed the type and thicknesses of the reaction and diffusion products without any assumptions as to the structure of the sample. The analysis could be pursued to a full quantification of the layer compositions given some additional information as to the heights of the same Auger features in elemental or

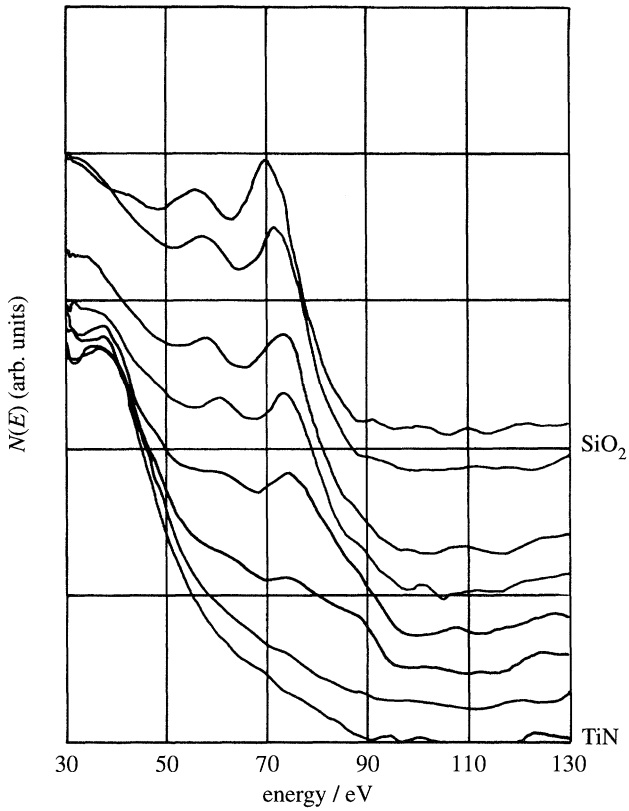

Figure 3. Spectra from regions of the bevel surface along a line perpendicular to the interfaces revealed by the bevelling. Incident beam 20 keV, 4 nA focused into a 100 nm diameter spot. Angle of incidence 32°. Take-off angle to the concentric hemispherical spectrometer 32°. Spectrometer pass energy 200 eV.

compound standards of known composition and an iterative matrix calculation of the kind described by Briggs & Seah (1990).

4. Principal component analysis

Principal component analysis (PCA) is a linear operation performed on data sets which finds linear combinations of the individual members of the set that are mutually orthonormal and ranked in order of decreasing variance. It is described in many books on data and image processing. In the case of image-spectra, one variant of the method is to find a new set of linear combinations of the original images—the principal component images—which are statistically independent of each other and ordered in a sequence of decreasing variance in each PC image. This matrix operation is carried out by computing the correlation or the covariance matrix of the image set, finding its eigenvalues and eigenvectors and forming the PC images by matrix multiplication of the original images with the eigenvectors which have been sorted to be in order of decreasing eigenvalue. Because there are usually fewer significant contrast mechanisms than there are images in the original data set, there are fewer PC images which contain information than there are original images. Therefore, PCA can be used as a method for data compression. The PCA transformation amounts

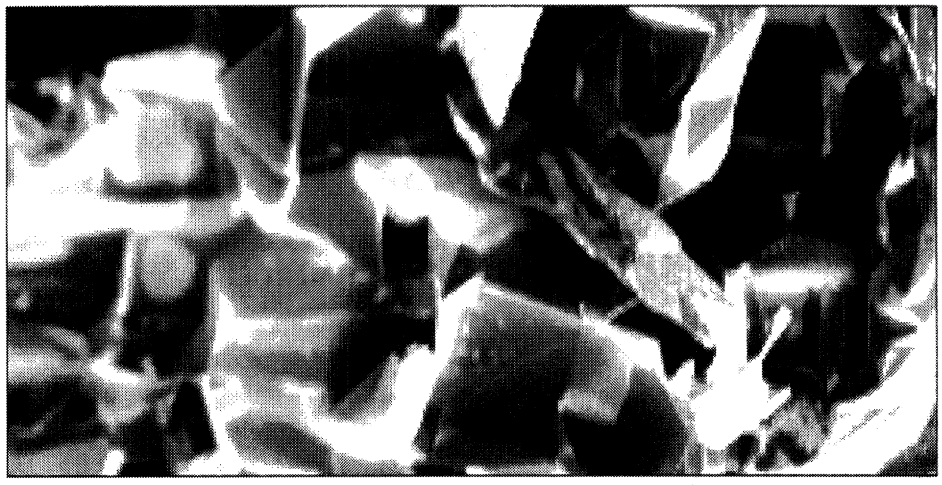

Figure 4. SEM image of a region of the PtRh catalyst sample. Incident beam 20 keV, 4 nA.

to a rotation of the N-dimensional scatter diagram so as to place the clusters with maximum separation along the first axis, the next greatest separation along the second axis and so on. The application of PCA (otherwise known as the eigenvector, the Hotelling or the Karhuenen–Loeve transform) to analytical electron microscopy has been described by Prutton *et al.* (1990).

As an example of the use of PCA, a sample of a used catalyst employed for the generation of HCN is chosen. This consists of a stack of 40 gauzes made from extruded Pt–Rh alloy wire. The surface is expected to contain Pt, Rh, N, C and O. During usage the wires are observed to facet massively and begin to coalesce as shown in the SEM image reproduced in figure 4. The objective of the study was to determine whether this sample had a surface composition which was uniform or varied from one facet to another.

Figure 5 shows the measured and processed Auger images for part of this surface. The severe roughness of the sample results in the contrast of the measured Auger images, *a*–*d*, being dominated by topographical artefacts (Holloway 1975; El Gomati *et al.* 1988). These are revealed in the correlations between the contrast in each of the four measured Auger images and it is difficult to make even a qualitative interpretation of the surface composition. The topographical artefacts were approximately removed from the measured Auger images by dividing them by an image collected simultaneously at 2400 eV (Crone *et al.* 1994). The result of this correction is shown in figure 5*e*–*h*. The corrected images are now clearly different to each other and are not all positively correlated. Nevertheless, the relationships between the images are complicated, particularly for N and O, the signals of which vary only slightly over this region of the surface. For this reason, PCA was applied in order to gain a better understanding of the situation.

The four principal component images are shown in figure 5*i*–*l* and their eigenvalues and eigenvectors are listed in table 1. Component 1 can be seen to be formed from the positive correlation of all four corrected images. This is interpreted as being due to incomplete correction of the topographical effects in the measured images. Component 2 is dominated by the anti-correlation between C and O, the image

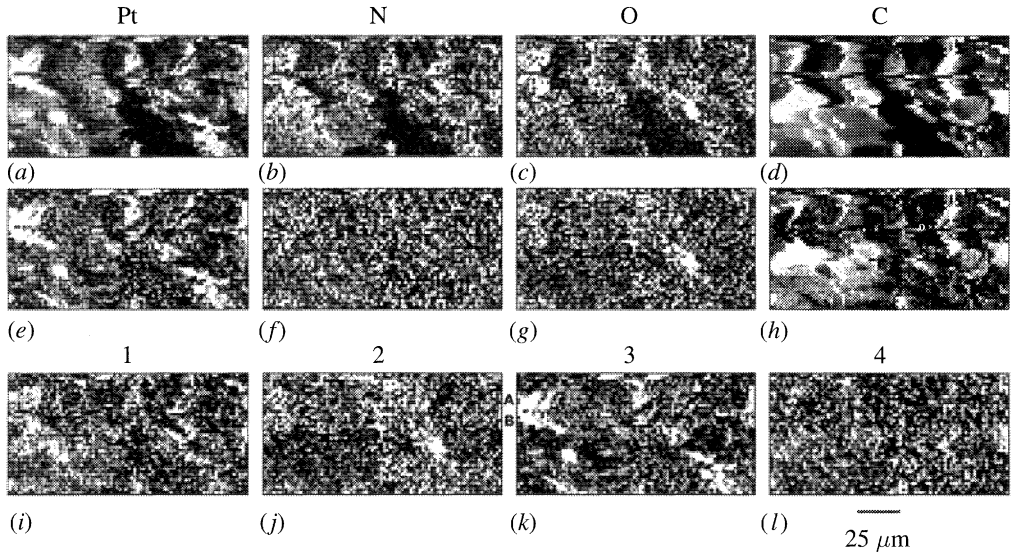

Figure 5. (*a*)–(*d*) show the measured Auger images and (*e*)–(*h*) the topography corrected Auger images for the very rough PtRh catalyst sample whose SEM image is shown in figure 4. Their four PC images are shown in (*i*)–(*l*). The eigenvectors and eigenvalues for the PC images are listed in table 1.

Table 1. *Eigenvalues and eigenvectors for a* PtRh *catalyst surface image set*

		eigenvector components			
component number	eigenvalues	Pt	N	C	O
1	1.28	0.399	0.666	0.579	0.251
2	0.99	−0.035	−0.019	−0.388	0.933
3	0.95	0.896	−0.140	−0.403	−0.124
4	0.76	0.192	−0.733	0.612	0.222

having higher intensities where O is high and C is low in concentration. This is particularly evident in the lower left-hand corner of each of these images. Component 3 maps places where the Pt concentration is high and the other three elements are all low. These high Pt regions correspond to particular facets of the sample. Two such facets (labelled A and B) can be seen in the top left-hand corner of the component 3 image. Component 4 maps regions where N is anti-correlated with the other elements. This particular phase would have been extremely difficult to identify from the corrected images alone.

Having carefully examined the component images, it is possible to inspect the corrected images and perceive the phases which have been identified. This observation would have been very difficult without the help of PCA.

PCA has been applied to other kinds of image sets obtained for 3D characterization of surfaces. An example of PCA applied to scanning tunnelling microscope images was first reported by Kenny *et al.* (1992) and has subsequently been used by Bouchard *et al.* (1994) to classify, with atomic resolution, the number of different

PHILOSOPHICAL TRANSACTIONS OF THE ROYAL SOCIETY A MATHEMATICAL, PHYSICAL & ENGINEERING SCIENCES

electronic species present at a surface. An interesting combination of ICP and PCA methodologies, which is called *recursive correlation partitioning*, has been demonstrated by King *et al.* (1990). Here, PCA is applied to the image set before ICP. After the major 'phases' have been partitioned, PCA is applied selectively to the remaining regions to further separate the contrast mechanisms. The process is repeated until all the 'phases' are distinguished.

5. Factor and target factor analysis

Thus far this paper has focused attention upon the manipulation of multi-image sets to extract useful information about the number and character of the various 'phases' present on a surface. However, the last step is always to obtain spectra in the places which have been defined as typical by the imaging experiments. The spectra then contain a wealth of information about the types of atoms, their bonding and environments. The methods of multivariate statistics are powerful here too. Gaarenstroom (1979, 1981, 1986) was the first to propose the application of PCA to sets of spectra measured as a surface is milled away with an ion beam. The objective in this case is to obtain a composition depth profile of the region of a solid immediately below its free surface. Once PCA has been applied, the related technique of target factor analysis (TFA) is then used. This finds the best (in the least squares fitting sense) linear combination of the standard elemental or compound spectra which will account for the raw spectra at each depth in the sample for which a measurement was made. Factor analysis (FA) is the combination of the two steps—PCA followed by TFA.

In principle, TFA should be capable of a quantitative analysis, in that atomic percentages of the standard spectra can be determined for each depth. Also, it should lead to greater precision of analysis because, instead of measuring peak heights or areas as in conventional quantification, the whole region of the spectra spanning the peaks of interest is used in the analysis. Theoretically, as more of the raw data are used to estimate the composition, better precision in the composition determination should be possible. This approach has been pursued and extended by several authors who have studied, for example, oxidation states at interfaces (Chemelli 1994; Kooi & Somers 1994), the composition of alloys with overlapping Auger features in their spectra (Calliari *et al.* 1994) and the analysis of carbides and nitrides (Reniers *et al.* 1994). It is an extremely powerful approach for the extraction of the maximum amount of useful information from a set of Auger spectra.

Kooi & Somers (1994) have an interesting reservation about the use of FA when analysing sets of spectra for which the raw data are in the form of a direct spectrum, EN(E). In this case, the Auger peaks are superimposed upon a slowly varying background due to the secondary electron cascade from the sample. This background can change shape, particularly at an interface region, as a sample is depth profiled between two layers of different materials. If FA is applied to the raw spectral data then extra significant factors (principal components) appear which have high loadings in the spectra localized near to the interface. Such 'ghost' components can be misinterpreted as additional chemical phases which are localized—perhaps by precipitation or segregation—at the interface. Kooi & Somers (1994) show that these ghost components arise from the change in shape of the secondary electron cascade in the region of the interface.

An example of such an effect has been found in the authors' laboratory in a study

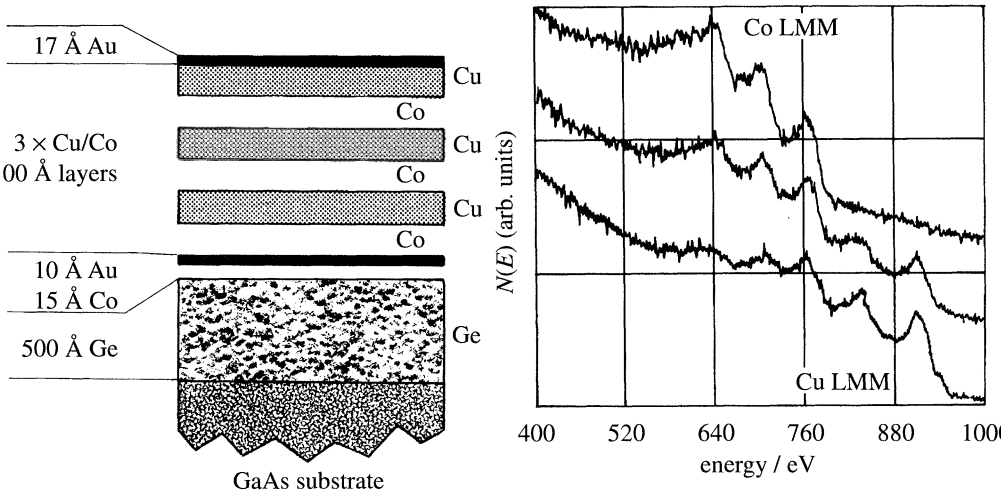

Figure 6. The structure of a bevelled CoCu multilayer sample and three of the spectra measured at different places in a single Co/Cu period in the sample.

of a multilayer CoCu sample. This material should be well suited to analysis by FA because there is overlap between the LMM Auger peaks of Cu and Co which can lead to difficulty in quantitative analysis by estimation of peak heights or areas. Figure 6 shows a cross-section through this sample after it had been bevelled with Xe^+ ions together with the three spectra measured at different positions across a single period of the CoCu multilayer. In all, 28 direct spectra were obtained across this cycle and the composition depth profile was calculated by applying TFA to these spectra as collected. The results are shown in figure 7. The noise in the profile is substantially lower than in the profile from a conventional quantification technique because all the information in the spectra has been used and not simply the peak heights. The layers are 10 nm thick and the ion beam mixing effects occurring during the bevelling process have reduced the depth resolution because this mixing has a depth scale of the order of 2–3 nm. Therefore, this would appear to be a most satisfactory result.

However, examination of the number of factors in the data set suggests that subtler effects are at work which may throw doubt upon the extent to which this depth profile can be trusted. The extent to which the variance in the data is accounted for is summarized in table 2. Since it is known that there are only two elements in the period of the structure, it might seem reasonable to anticipate that there would be two factors accounting nearly all the variance. In fact, table 2 indicates that three factors are required to account for the variance in the data set. The third factor, although small, is statistically significant, being caused by modifications to the inelastic losses of one set of Auger peaks as the electrons pass through the other material. This is another 'ghost' component similar to those found by Kooi & Somers (1994).

The secondary electron cascade can be removed by using subtraction of a power law form extrapolated from above the family of peaks followed by Peacock's (Peacock 1985) adaptation of Shirley's method for removal of the characteristic loss spectrum at energies below the Auger peaks. If TFA is then carried out, the variance in the processed data set which is accounted for by two factors is found to decrease to about 97% rather than to increase. This is attributed to systematic inaccuracies in the background removal algorithm. Much better algorithms based upon a physical

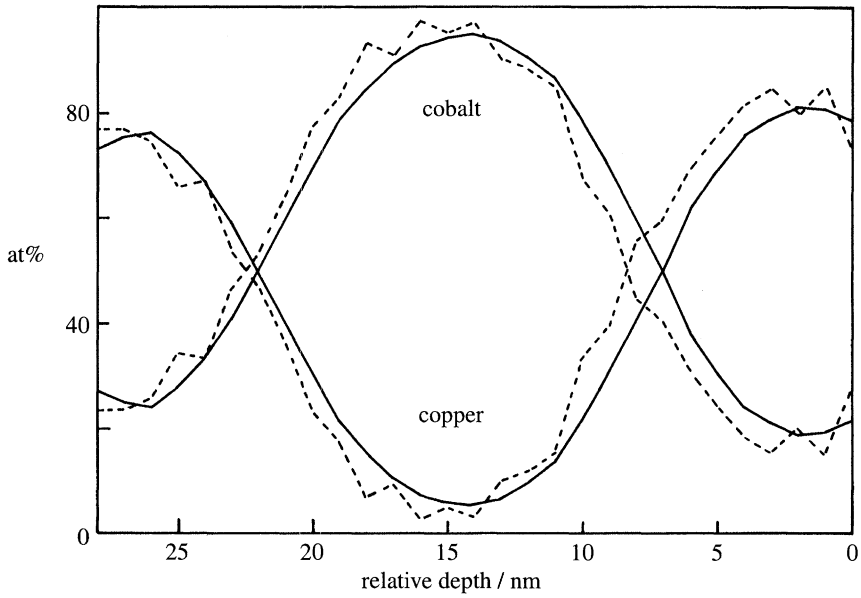

Figure 7. The depth profile calculated by TFA from 28 spectra measured along the bevel surface. The solid line is the depth profile calculated by TFA and the broken line shows the profile calculated from the peak heights using conventional quantification methods. Note that the depth scale is not referred to an origin at the surface. The systematic displacement of the TFA profile to greater thicknesses may be a consequence of the use of the differentiated spectra for the conventional quantification and the (background stripped) direct spectra for the TFA calculation. These two signals may have different surface sensitivities.

Table 2. *Target factor analysis for one period of* CoCu *multilayer with* 10 nm *thick layers*

factors number	variance accounted for by extra factor (%)
1	99.5967
2	0.3580
3	0.0163
4	0.0016
5	0.0015

description of the energy loss spectrum are now available (Tougaard 1984, 1989) but these remain to be tested in the context of TFA.

6. Discussion and conclusions

Chemometrics is a well established discipline in which mathematical and statistical methods are used to handle, interpret and predict chemical data. The material outlined here marks the beginning of a daughter discipline which might be called *surface chemometrics*. It is not simply a statistical approach to the analysis of the results of surface sensitive experiments. Rather, it seeks to combine the physics of the electron–solid (or ion–solid or photon–solid) interaction with statistical treatment of sets of data. This paper has sought to illustrate some of the means by which this can

be achieved by taking examples from scanning Auger microscopy and Auger spectroscopy, but other spectroscopies are yielding related and sometimes complementary results.

The surface chemometric approach has been particularly successful in scanning Auger microscopy because it has provided means for combining the signals produced by several different detectors in a way which helps to eliminate artefacts in image contrast arising from topography and electron backscattering. This has led to the possibility of studying the surfaces of rough, heterogeneous materials for the first time. Since the surfaces of VLSI integrated structures are important examples of rough and heterogeneous systems, this kind of multi-imaging electron microscopy holds considerable promise for the future micro and nano analysis of these materials.

Multi-imaging strategies have commenced in SIMS, EDX and photo-emission spectroscopies and it seems reasonable to predict that these techniques will also show considerable growth as the appropriate hardware and software tools become available.

The authors thank the Engineering and Physical Sciences Research Council for the support of both the MULSAM project and two of the authors (I.R.B. and M.W.) at York and the Deep Multispectral Imaging project at Bradford (P.G.K.). We also thank the coordinators and collaborators in the ADEQUAT phase 2 component of the EU's ESPRIT III programme for their support of R.H.R. and the samples used in the scatter diagram, ICP, study outlined above. The $W/TiN/Ti/SiO_2$ metallization sample was provided as part of this collaboration by K. Stribley of GEC Plessey Semiconductors Ltd.; the PtRh catalyst sample was kindly provided by Dr D. Briggs and Dr S. Axon of ICI plc; the CuCo layer sample was kindly provided by Professor D. Greig, Department of Physics, University of Leeds.

References

Barkshire, I. R., Prutton, M., Greenwood, J. C. & Kenny, P. G. 1992 Correction of topographical artefacts in Auger images using four backscattered electron detectors. *Appl. Surf. Sci.* **55**, 245–255.

Bonnet, N. 1995 Preliminary investigation of methods for the automatic handling of multivariate maps in microanalysis. *Ultramicroscopy* **57**, 19–27.

Bouchard, A. M., Osbourn, G. C. & Swartzentruber, B. S. 1994 New method for empirically determining surface electronic species from multiple-bias STM images: a multivariate classification approach. *Surf. Sci.* **321**, 276–286.

Briggs, D. & Seah, M. P. 1990 *Practical surface analysis.* Chichester: Wiley

Bright, D. S. Newbury, D. E. & Marinenko, R. B. 1988 Concentration-concentration histograms: scatter diagrams applied to quantitative compositional maps. In *Microbeam analysis* (ed. D. E. Newbury), pp. 18–24. San Francisco, CA: San Francisco Press.

Bright, D. S. & Marinenko, R. B. 1992 Concentration histogram imaging: a quantitative view of related images. In *Microscopy: the key research tool*, vol. 22, pp. 21–28. Milwaukee: Electron Microscope Society of America.

Browning, R. 1985 Ratioed scatter diagrams. An erotetic method for phase identification on complex surfaces using scanning Auger microscopy. *J. Vac. Sci. Technol.* A **3**, 1959–1963.

Calliari, L., Gonzo, L., Micheli, V. & Tiscione, P. 1994 Auger quantitative analysis of brass via target factor analysis. *Surf. Interface Analysis* **21**, 571–575.

Chemelli, G. 1994 Chemical information from Auger data using factor analysis: some examples. *Surf. Interface Analysis* **22**, 60–64.

Crone, M., Barkshire, I. R. & Prutton, M. 1994 New technique for the simultaneous correction of topographical and backscattering artefacts in electron-excited Auger spectroscopy and imaging. *Surf. Interface Analysis* **21**, 857–863.

PHILOSOPHICAL TRANSACTIONS OF THE ROYAL SOCIETY A MATHEMATICAL, PHYSICAL & ENGINEERING SCIENCES

El Gomati, M. M., Peacock, D. C., Prutton, M. & Walker, C. G. H. 1987 Scatter diagrams in energy analysed digital imaging: application to scanning Auger microscopy. *J. Microscopy* **147**, 149–158.

El Gomati, M. M., Prutton, M., Lamb, B. & Tuppen, C. G. 1988 Edge effects and image contrast in scanning Auger microscopy: a theory–experiment comparison. *Surf. Interface Analysis* **11**, 251–265.

Gaarenstroom, S. W. 1979 Chemical characterisation from Carbon Auger spectra by application of pattern recognition and factor analysis. *J. Vac. Sci. Technol.* **16**, 600–604.

Gaarenstroom, S. W. 1981 Principal component analysis of Auger line shapes at solid–solid interfaces. *Appl. Surf. Sci.* **7**, 7–18.

Gaarenstroom, S. W. 1986 Application of factor analysis to elemental detection limits in sputter depth profiling. *Appl. Surf. Sci.* **26**, 561–574.

Gonzalez, R. C. & Wintz, P. 1982 *Digital image processing.* Reading, MA: Addison-Wesley.

Holloway, P. H. 1975 The effect of surface roughness for Auger electron spectroscopy. *J. Electron Spectrosc. Rel. Phen.* **7**, 215–232.

Kenny, P. G., Prutton, M., Roberts, R. H., Barkshire, I. R., Greenwood, J. C., Hadley, M. J. & Tear, S. P. 1992 The application of multispectral techniques to analytical electron microscopy. *Scanning Electron Microscopy Suppl.*, vol. 6, pp. 361–367. Chicago, IL: Scanning Microscopy International.

Kenny, P. G., Barkshire, I. R. & Prutton, M. 1994 Three-dimensional scatter diagrams: application to surface analytical microscopy. *Ultramicroscopy* **56**, 289–301.

King, P. L., Browning, R., Pianetta, P., Lindau, I., Keenlyside, M. & Knapp, G. 1989 Image processing of multispectral XPS images. *J. Vac. Sci. Technol.* A **7**, 3301–3306.

King, P. L., Browning, R., Paque, J. M. & Pianetta, P. 1990 EDS image classification by projection after partitioning. In *Proc. XIIth Int. Cong. for Electron Microscopy* (ed. L. D. Peachey & D. B. Williams), vol. 1, pp. 464–465. San Francisco, CA: San Francisco Press.

Kooi, B. J. & Somers, M. A. J. 1994 Factor analysis of Fe $M_{2,3}VV$ spectra of oxidizing iron: the role of the background in the emergence of ghost components. *Surf. Interface Analysis* **21**, 501–513.

Krivanek, O. L., Delby, N., Gubbens, A. J., Kundmann, A. K., Leber, M. I., Ray, D. A. & Truong, K. V. 1990 Advances in parallel-detection EELS. In *Proc. XIIth Int. Cong. for Electron Microscopy*, vol. 2, pp. 76–77. San Francisco, CA: San Fransisco Press.

Malinowski, E. R. 1991 *Factor analysis in chemistry.* Chichester: Wiley.

Meloun, M., Militky, J. & Forina, M. 1992 *Chemometrics for analytical chemistry.* Chichester: Ellis Horwood.

Niblack, W. 1986 *Digital image processing.* Englewood Cliffs, NJ: Prentice Hall.

Peacock, D. C. 1985 Fitting the inelastic tail below experimentally observed Auger peaks. *Surf. Sci.* **152–153**, 895–899.

Prutton, M., El Gomati, M. M. & Kenny P. G. 1990 Scatter diagrams and Hotelling transforms: application to surface analytical microscopy. *J. Electron Spectrosc. Rel. Phen.* **52**, 197–219.

Prutton, M., Walker, C. G. H., Greenwood, J. C., Kenny, P. G., Dee, J. C., Barkshire, I. R., Roberts, R. H. & El Gomati, M. M. 1991 A third generation Auger microscope using parallel multispectral data acquisition and analysis. *Surf. Interface Analysis* **17**, 71–84.

Reniers, F., Hubin, A., Terryn, H. & Vereecken, J. 1994 Factor analysis as a tool to deconvolute Auger spectra of tungsten nitrides and carbides. *Surf. Interface Analysis* **21**, 483–489.

Schueler, B. 1990 In *Secondary ion mass spectroscopy, SIMS VII* (ed. A. Benninghoven, C. A. Evans, K. D. McKeegan, H. A. Storms & H. W. Werner), pp. 311–314. Chichester: Wiley.

Tougaard, S. 1984 Deconvolution of loss features from electron spectra. *Surf. Sci.* **139**, 208–218.

Tougaard, S. 1989 Practical algorithm for background subtraction. *Surf. Sci.* **216**, 343–360.

PHILOSOPHICAL TRANSACTIONS OF THE ROYAL SOCIETY A MATHEMATICAL, PHYSICAL & ENGINEERING SCIENCES

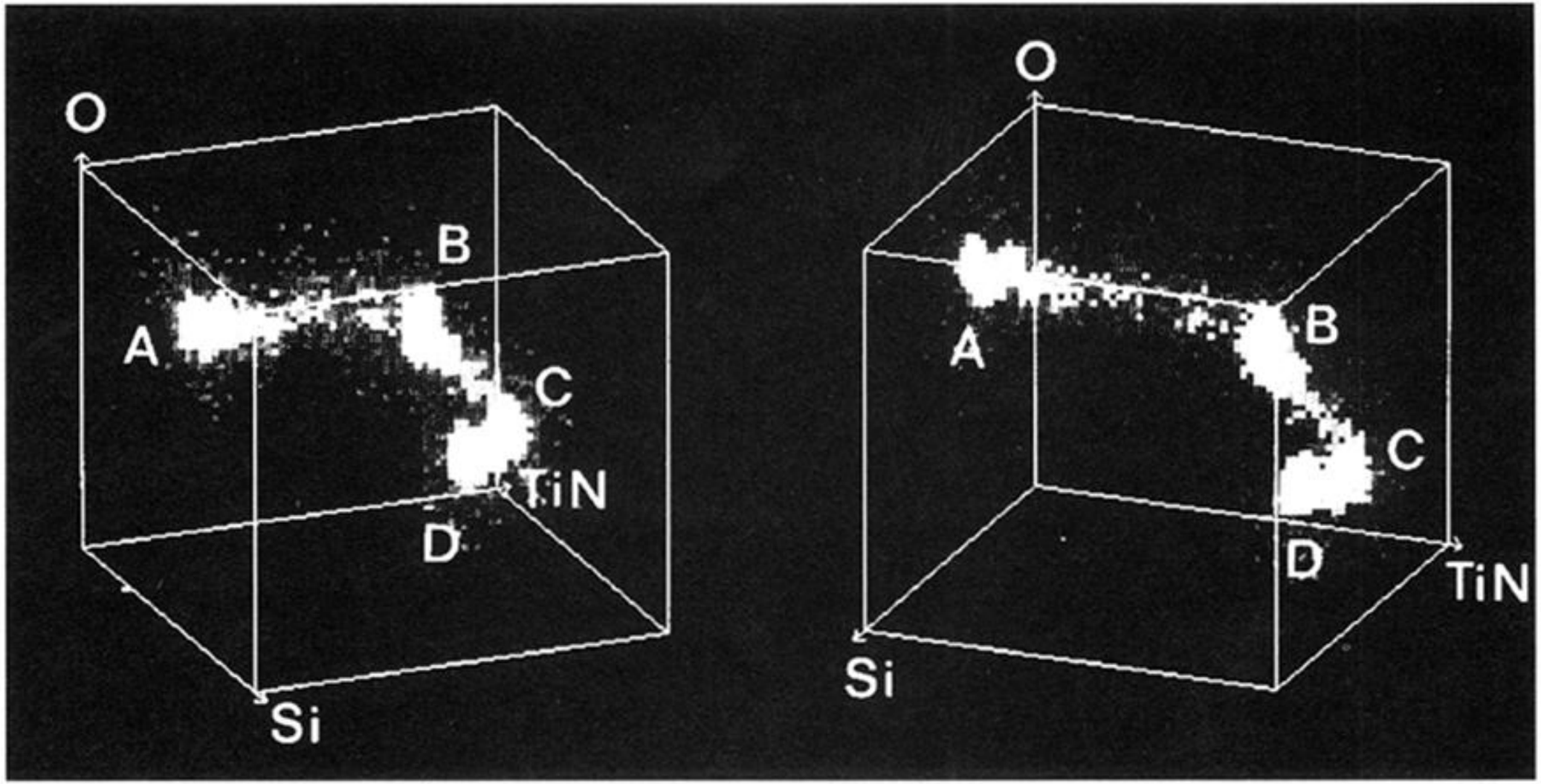

igure 1. Two projections of the 3D scatter diagram formed from the O, Ti/N and Si peaks escribed in the text. Clusters A–D contain the largest numbers of pixels and the remaining usters appear on the correlation streak between clusters A (SiO_2) and B (a mixture of Ti and peaks)

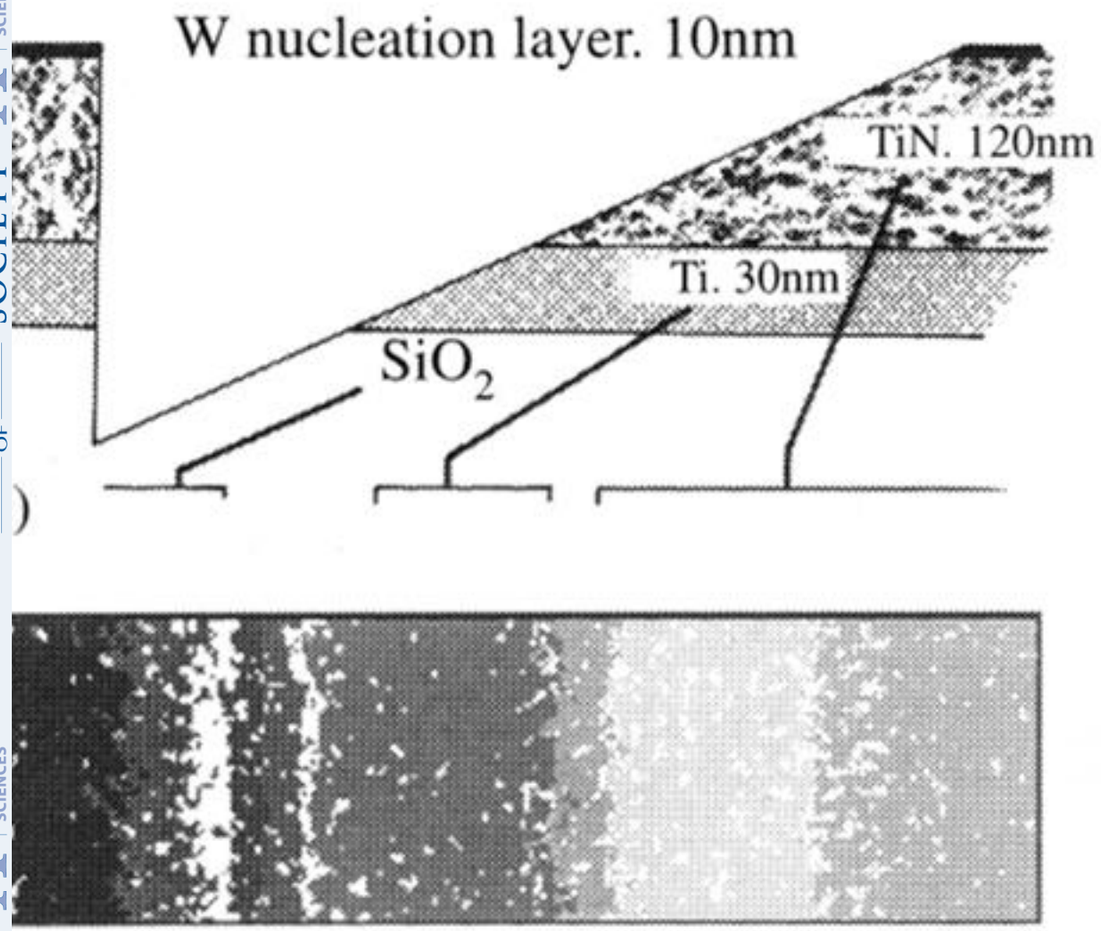

)

?)

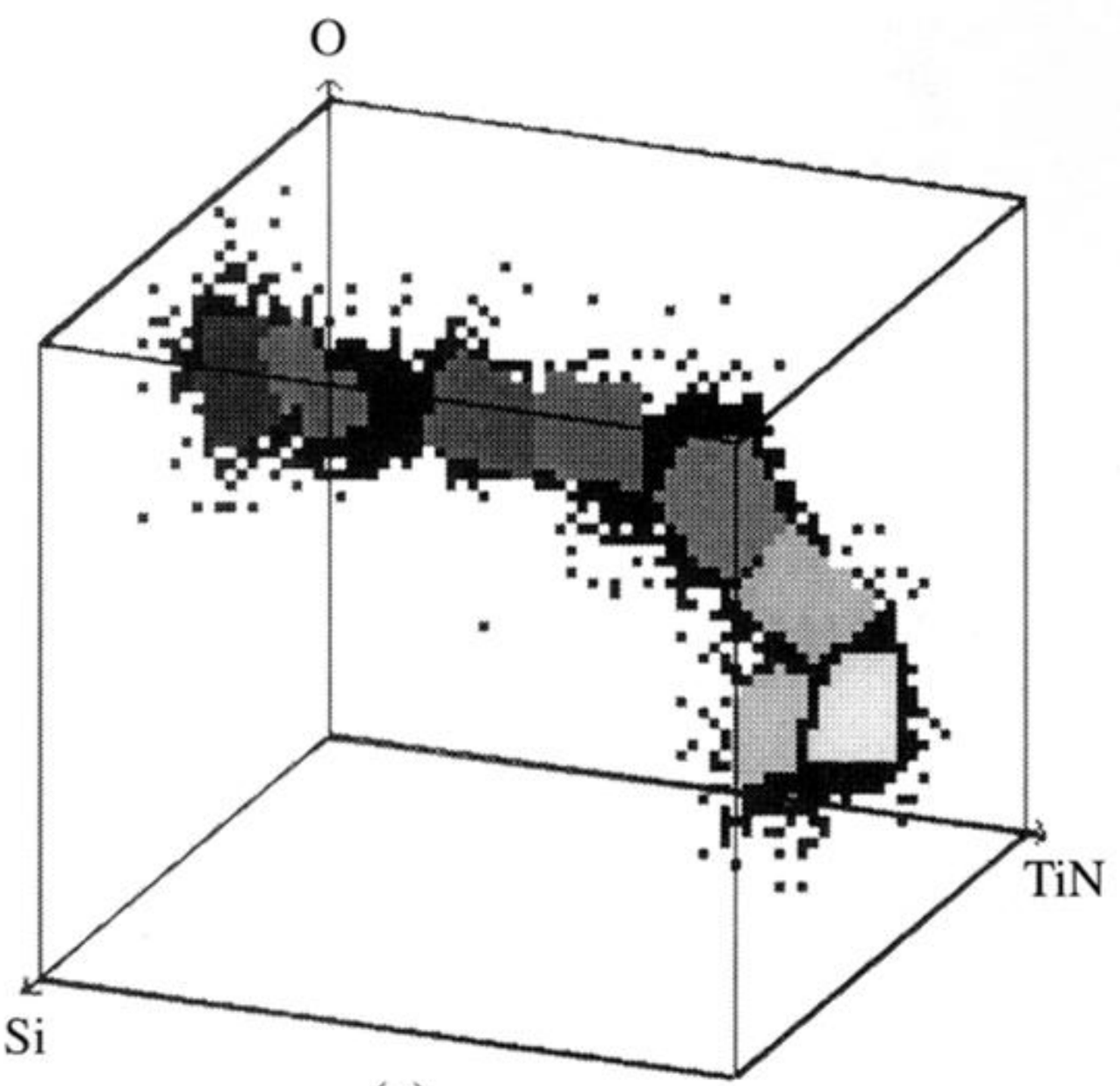

(*c*)

gure 2. (*a*) Cross-section through the structure which was expected in the sample, the data of hich are presented in figures 1 and 3. (*b*) False colour image derived from the scatter diagram figure 1 together with the scatter diagram which indicates the assignment of false colours each cluster. Normally the false colour image is in colour but, for reasons of economy, it is produced here in a grey scale.

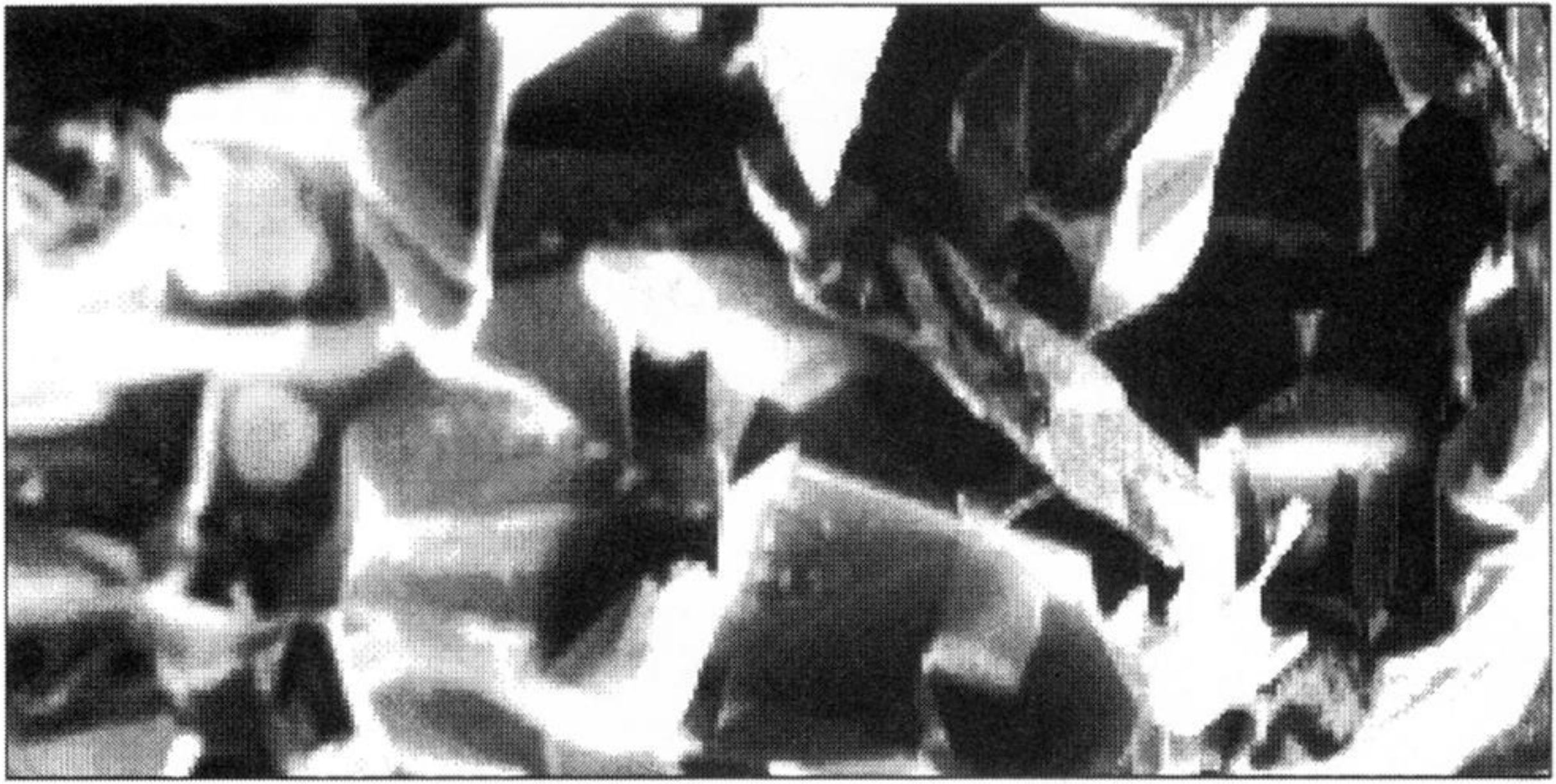

gure 4. SEM image of a region of the PtRh catalyst sample. Incident beam 20 keV, 4 nA.

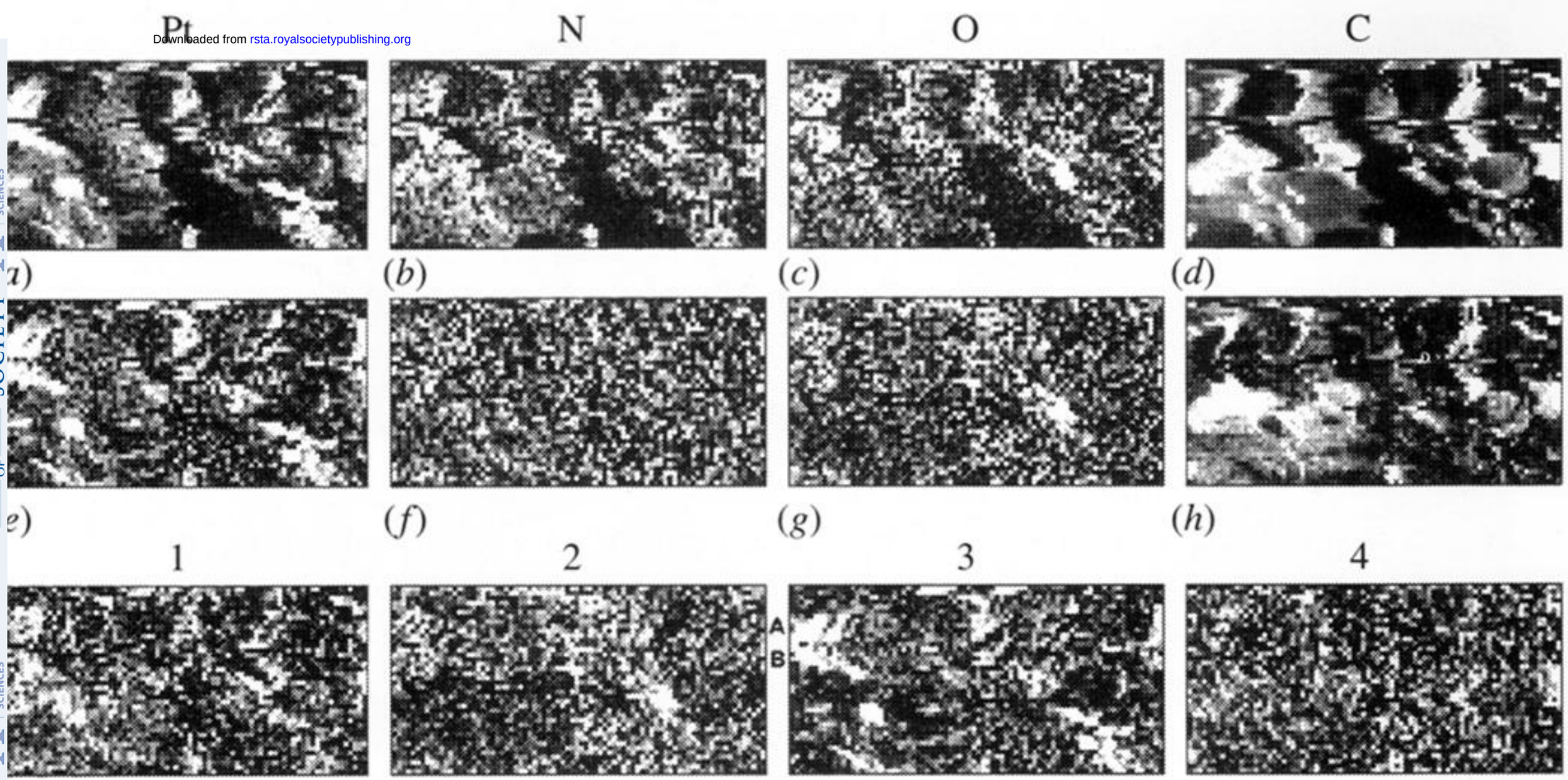

Figure 5. (*a*)–(*d*) show the measured Auger images and (*e*)–(*h*) the topography corrected Auger images for the very rough PtRh catalyst sample whose SEM image is shown in figure 4. Their four PC images are shown in (*i*)–(*l*). The eigenvectors and eigenvalues for the PC images are listed in table 1.